Plasma-induced defects engineering of porous metal–organic framework nanosheet arrays for efficient water splitting

Junnan Song,[a,b] Sheng Zhao,[b] Di Liu,[c] Yixing Xiong,[b] Feng Hu,[b] Linlin Li,[b] Lei Li,*[a] Hui Pan,*[c] Shengjie Peng*[b]

[a.] *College of Biological, Chemical Sciences and Engineering, Jiaxing University, Jiaxing, Zhejiang 314001, China. E-mail: leili@mail.zjxu.edu.cn*
[b.] *College of Materials Science and Technology, Nanjing University of Aeronautics and Astronautics, Nanjing 210016, China. E-mail: pengshengjie@nuaa.edu.cn*
[c.] *Institute of Applied Physics and Materials Engineering, University of Macau, Macao SAR. E-mail: huipan@um.edu.mo*

Experimental

Chemicals

Terephthalic Acid (H_2BDC), iron (III) chloride hexahydrate ($FeCl_3 \cdot 6H_2O$), dimethyl formamide (DMF), hydrochloric acid (HCl), and absolute ethyl alcohol purchased from Aladdin were used directly without further purification.

Synthesis of Fe MOF/IF

Fe MOF/IF nanosheet arrays were prepared by following a simple hydrothermal method. Specifically, 0.127 g H_2BDC and 0.413 g $FeCl_3 \cdot 6H_2O$ were dissolved in the mixed solution of DMF (32 mL), ultrapure water (1 mL), HCl (1 mL), and absolute ethyl alcohol (2 mL). After complete dissolution, the mixed solution was transferred into a 50 mL Teflon-lined autoclave. Subsequently, a piece of commercial Fe foam (IF, 3×3 cm^2) was introduced into the above mixed solution and maintained at 140 ºC for 12 h (The IF substrates were ultrasonically washed with deionized water and ethanol several times to clean the surface impurities, then put them into 6.0 M HCl solution for 5 min to remove the surface oxide layers, and rinsed subsequently with water and

ethanol, finally dried in vacuum). After that, the products were washed with ultrapure water and ethyl alcohol sever times and dried at 60 ºC overnight in vacuum. The obtained self-supporting sample was labelled as Fe MOF/IF.

Synthesis of O_v-Fe MOF/IF

The O_v-Fe MOF/IF was obtained by treating the pristine Fe MOF/IF with N_2 plasma. RF power of 200 W, the pressure of 3 Pa, a suitable bias voltage, and an N_2 flow rate of 80 sccm were employed for the plasma treatment. For comparison, a series of comparative samples with different irradiation time (10, 20, and 30 min) have been synthesized, and the obtained samples were denoted as O_v-Fe MOF/IF-10min, O_v-Fe MOF/IF-20min, and O_v-Fe MOF/IF-30min, respectively.

Characterization

Morphology and microstructure of samples were observed via field-emission scanning electron microscope (FESEM, Regulus 8100) and transmission electron microscope (TEM, FEI Tecnai G2 F20) as well as high resolution TEM (HRTEM). TEM mapping was also conducted on FEI Tecnai G2 F20. The Brunauer–Emmett–Teller (BET) surface area was determined using nitrogen adsorption-desorption carried by the Surface Area (V-Sorb 2800P, Gold APP Instruments, China). The phase structures were characterized by X-ray diffractometer (XRD, Bruker D8 ADVANCE). The elemental composition and chemical state were confirmed by X-ray photoelectron spectroscopy (XPS Escalab 250Xi). The Raman measurements were accomplished by a Raman micro spectrometer (Thermo Fischer DXR) with 532 nm of excitation. The electron paramagnetic resonance (EPR) data was tested by the Bruker A300 in N_2 test mode. X-ray absorption fne structure spectra were measured under room temperature using the transmission mode of the XAFCA beamline in the Singapore Synchrotron Light Source. Extended X-ray absorption fine structure data was interpreted utilizing WINXAS 3.1 code, where it was normalized and then transformed to momentum space (k) from the initial energy space. The chemical states of the materials were studied by X-ray photoelectron spectroscopy (Thermo ESCALAB 250).

Electrochemical measurements

All electrochemical measurements were performed on an electrochemical workstation (Autolab PGSTAT302, Eco Chemie, Netherlands) with a conventional three-electrode electrochemical cell system, in which the graphite rod and platinum foil were used as the counter electrode, as-prepared samples were directly used as the working electrodes, and Ag/AgCl was used as the reference electrode. The estimated electrochemical double layer capacitances (C_{dl}) were obtained by cycle curves (CV) tests in a non-Faradaic potential region at different scan rates of 1, 2, 5, 10, 20, 30, 40 and 50 mV s^{-1}. All of the polarization curves were recorded via linear sweep voltammetry (LSV) measurements at a scanning rate of 5 mV s^{-1} and were recorded with iR compensation. And all the potentials were referenced to RHE according to the Nernst equation:

$$E_{RHE} = E_{Ag/AgCl} + 0.198 + 0.0591 \times pH$$

The electrochemical impedance spectroscopy (EIS) was conducted over the frequency range of 0.01–105 kHz with an amplitude of 10 mV. The stability was tested at a constant current density of 10 mA cm^{-2} in 1.0 M KOH. The overall water splitting was conducted in a single-compensation cell, with the as-obtained electrodes as the working electrode and the counter electrode.

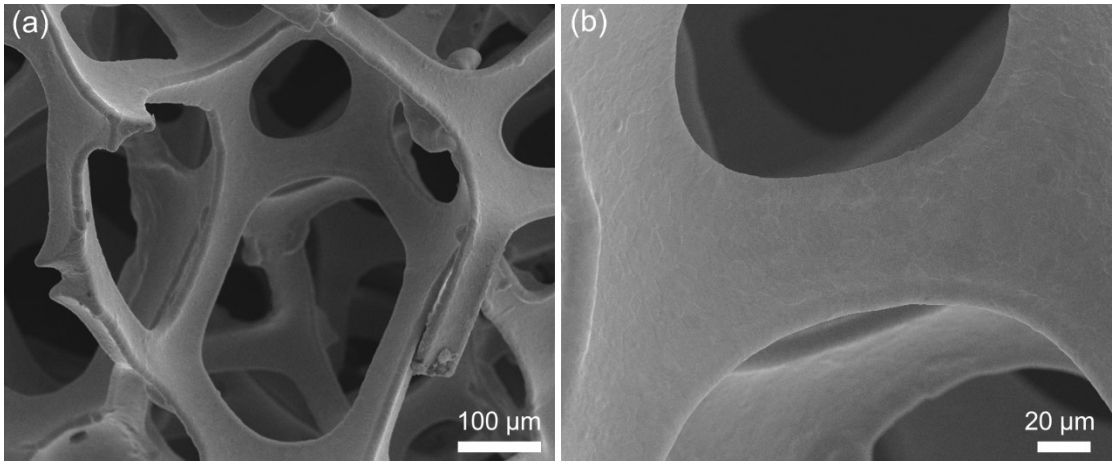

Fig. S1 a) Low-magnified and b) high-magnified SEM images of bare IF.

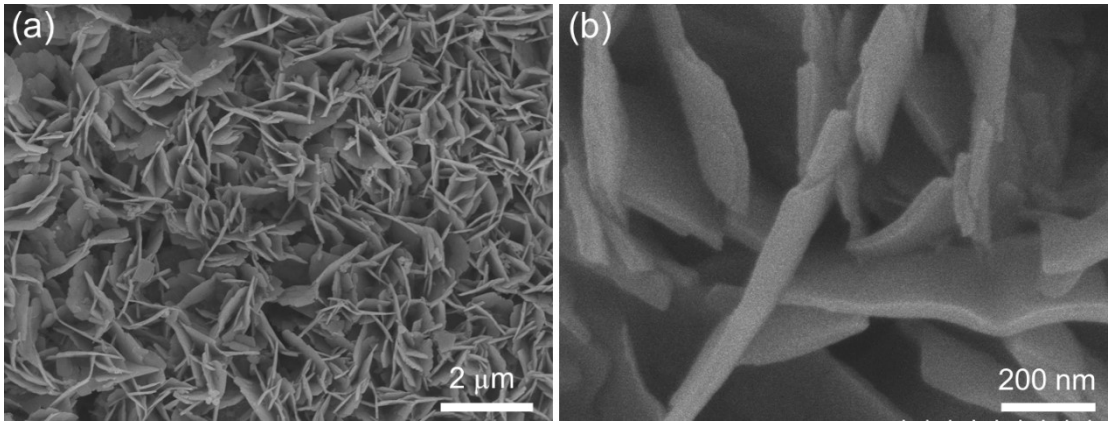

Fig. S2 a) Low-magnified and b) high-magnified SEM images of pristine Fe MOF/IF nanosheets, respectively.

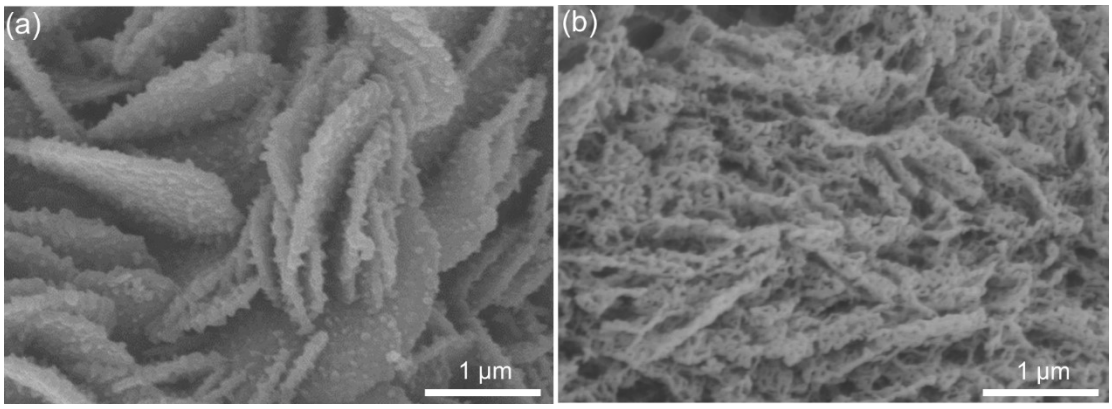

Fig. S3 SEM images of Fe MOF/IF nanosheets treated by plasma for a) 10 min and b) 30 min at 200 W.

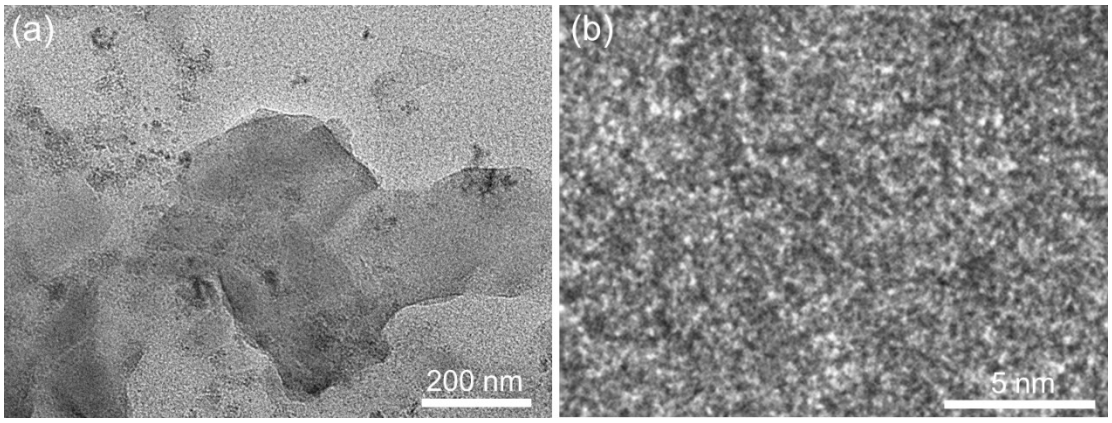

Fig. S4 a) TEM and b) HRTEM images of pristine Fe MOF/IF nanosheets, respectively.

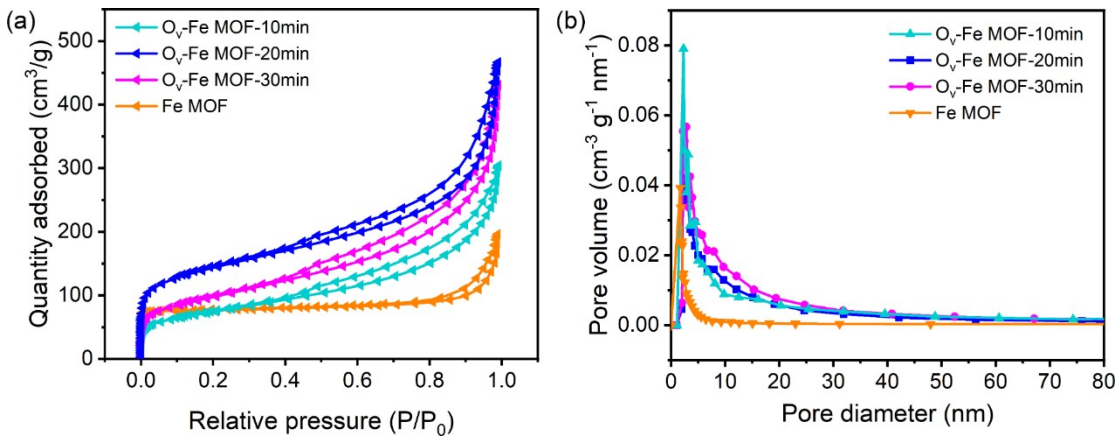

Fig. S5 a) Nitrogen adsorption and desorption curves, and b) size distribution plots of O_v-Fe MOF/IF and pristine Fe MOF/IF nanosheets.

The BET specific surface area of materials was obtained by measuring the MOF powder scraped from the Fe foam substrate. The specific surface area of O_v-Fe MOF/IF samples was calculated to be 262.85 m^2 g^{-1} for O_v-Fe MOF/IF-10min, 502.51 m^2 g^{-1} for Ov-Fe MOF/IF-20min, and 347.56 m^2 g^{-1} for O_v-Fe MOF/IF-30min, which are higher than that of pristine Fe MOF (112.51 m^2 g^{-1}), demonstrating the plasma treatment could effectively increase the surface area of Fe MOF. Additionally, both BJH median pore width and SF median pore width show an increasing trend with the extension of plasma processing time (**Table S1**).

Table S1. Parameters of BJH median pore width and SF median pore width of Fe MOF with different plasma treatment time.

Samples	BJH median pore width (nm) [a)]	SF median pore width (nm) [b)]
Fe MOF	9.294	0.703
Ov-Fe MOF/IF-10min	9.849	0.743
Ov-Fe MOF/IF-20min	10.133	0.737
Ov-Fe MOF/IF-30min	27.102	1.169

a) Barnes-Jewish Hospital (BJH) adsorption median pore width

b) Saito-Foley (SF) median pore width

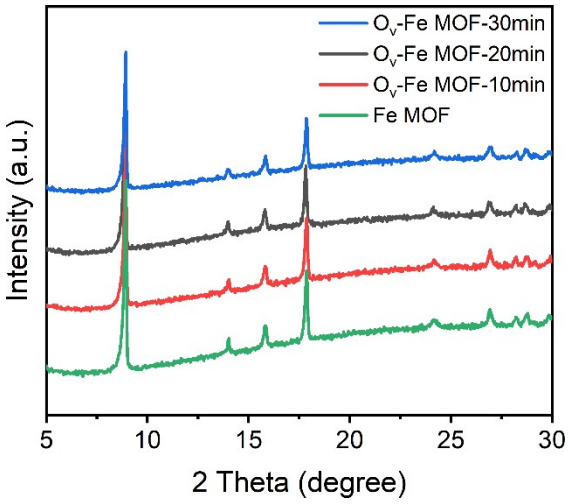

Fig. S6 XRD patterns of pristine Fe MOF/IF and O_v-Fe MOF/IF nanosheets.

The structure of Fe MOFs is consistent with MIL-53 (Adv. Energy Mater. 2018, 8, 1800584.), in which Fe ions are coordination centers and linked by terephthalic acid.

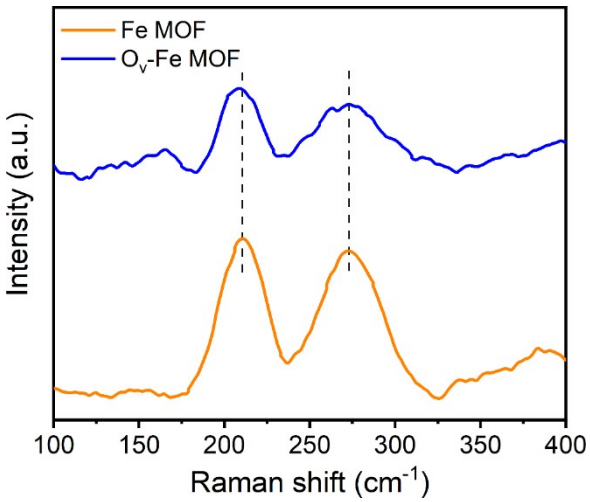

Fig. S7 Raman spectra of pristine Fe MOF/IF and O_v-Fe MOF/IF nanosheets.

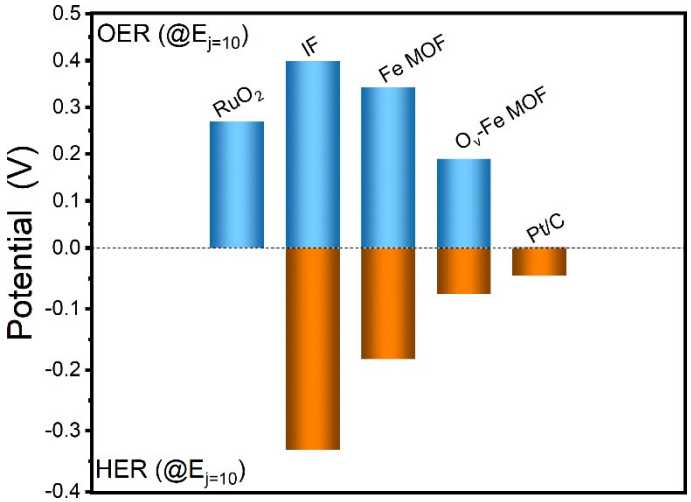

Fig. S8 The overall performance comparison histogram for all catalysts by ΔE (The potential gap between HER and the OER potential at 10 mA cm^{-2}).

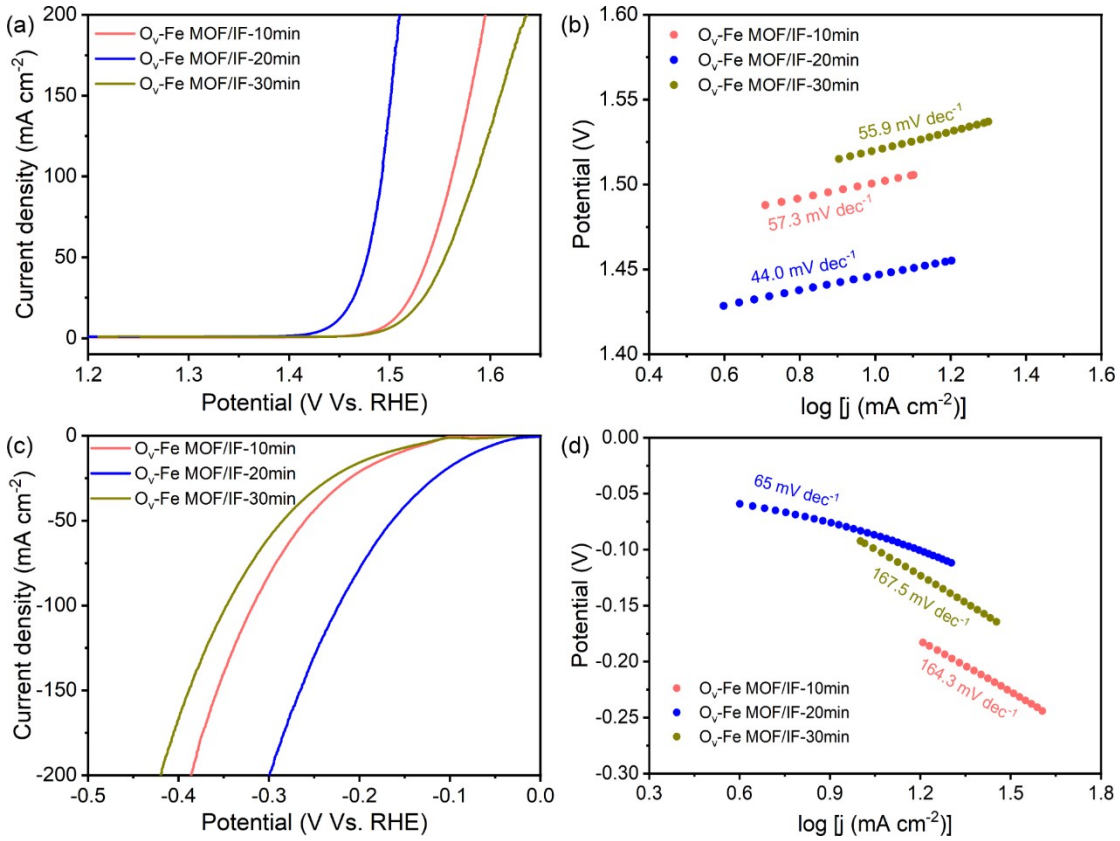

Fig. S9 Catalytic performance of Fe MOF/IF nanosheets treated by plasma for different time towards for a and b) OER and c and d) HER. a, c) The polarization curves and b, d) Tafel plots.

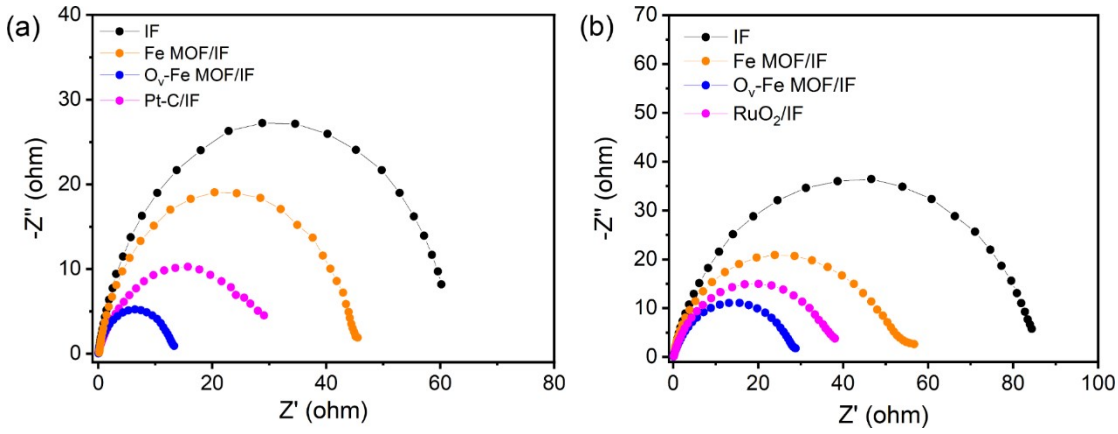

Fig. S10 a) HER and b) OER EIS spectra of pristine IF, Fe MOF/IF, O_v-Fe MOF/IF, and Pt/C/IF catalysts, respectively.

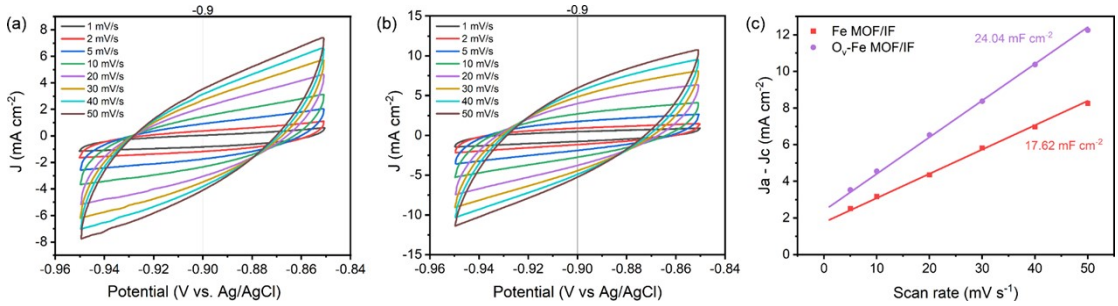

Fig. S11 CV curves measured at different scans for a) Fe MOF/IF, and b) O_v-Fe MOF/IF. c) C_{dl} evaluation for Fe MOF/IF and O_v-Fe MOF/IF.

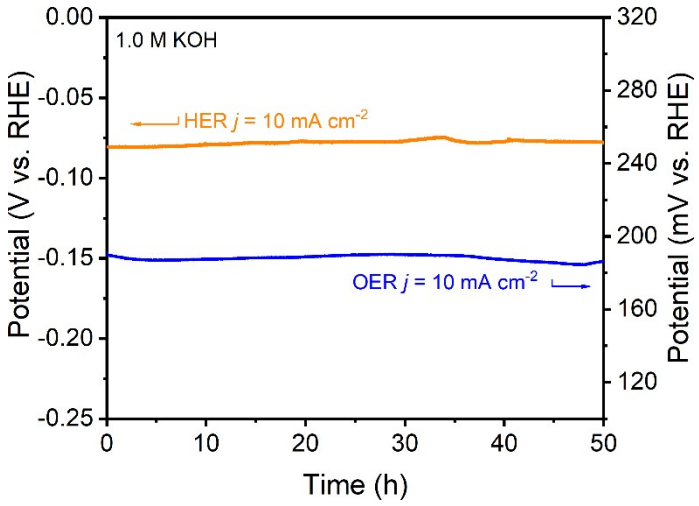

Fig. S12 Chronoamperometric curves of O_v-Fe MOF/IF toward OER and HER.

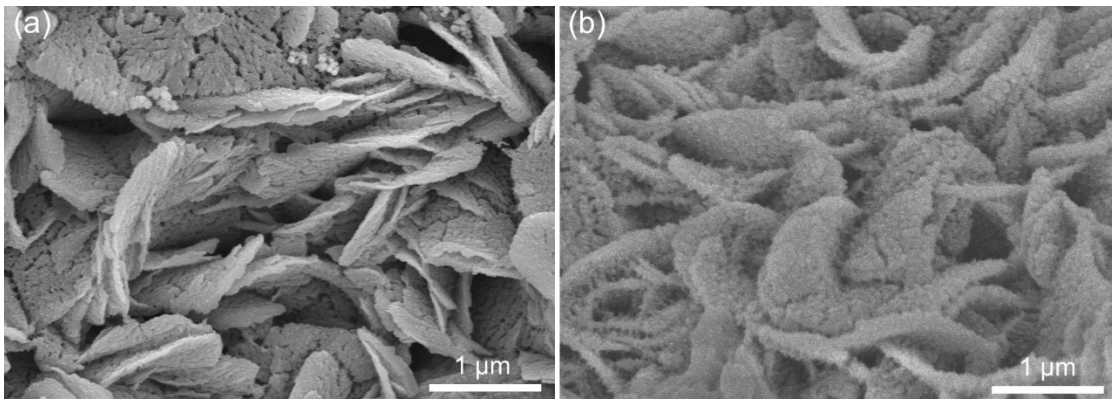

Fig. S13 SEM images of O_v-Fe MOF/IF nanosheets after a) HER and b) OER test.

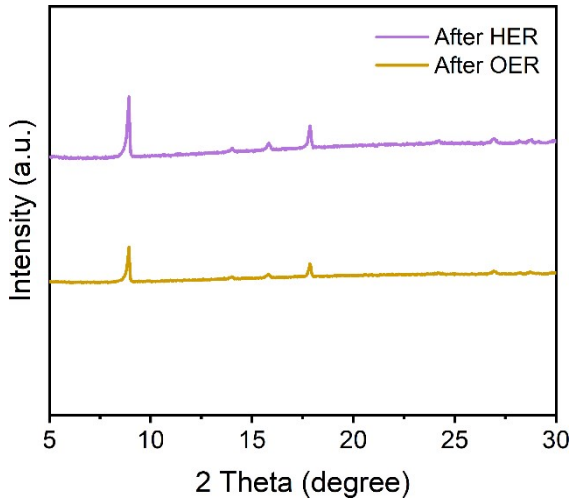

Fig. S14 XRD patterns of O_v-Fe MOF/IF nanosheets after water splitting test.

Table S2. Comparison of MOF-based catalysts for electrocatalytic OER in 1 M KOH in recent publications.

Catalysts	**ηOER_{10} (mV)**	**Ref.**
O_v-Fe MOF/IF	**200**	**This work**
NiFe-MS/MOF@NF	230@50	Adv. Sci. 2020, 7, 2001965.
FeNi(BDC)(DMF,F)	227@60	Appl. Catal. B: Environ. 2019, 258, 118023.
CoP/D-CoCu-MOF-300	295	J. Mater. Chem. A, 2020, 8, 14099–14105.
CoCu-MOF NBs	271	Angew. Chem. Int. Ed. 2021, 60, 26397–26402.
IrO_2@IrMOF-ppy	207	J. Mater. Chem. A, 2020, 8, 25687–25695.
a_gZIF-62(Co)-Fe-CC	256	Angew. Chem. Int. Ed. 2022, 61, 202112880.
Ni@CoO@CoMOFC	247	J. Mater. Chem. A, 2021, 9, 22597–22602.
defect-Ni-MOF	219	Small 2020, 16, 1906564.
2D Ni-MOF-250	250@50	J. Mater. Chem. A, 2020, 8, 2140–2146.
2D MOF-Fe/Co	238	Angew. Chem. 2021, 133, 12204 – 12209.
Ru/NiFe$(OH)_x$/NiFe-MOF	242	J. Mater. Chem. A, 2021, 9, 24670–24676.
NiFc-MOF/NF	195	Angew. Chem. 2021, 133, 12880 –12884.
Ir-Ni-NS	270	Adv. Mater. Interfaces 2021, 8, 2002034.
cMOF/LDH	216@50	Adv. Mater. 2021, 33, 2006351.
MCCF/NiMn-MOFs	280	Angew. Chem. Int. Ed. 2020, 59, 18234 –18239.
Ni-doped FeF_2	275	Chem. Commun., 2020, 56, 7889—7892.
Fe–Ni LDH/MOF-b2	255	Nanoscale, 2020, 12, 14514–14523.
$Ni_{0.9}Fe_{0.1}$-MOF	198	Nature Energy 2020, 5, 881–890.
3D Ni-MOF/NF	350	Inorg. Chem. Front., 2021, 8, 3007–3011.
Br-Ni-MOF	306	Sci. Adv. 2021, 7, eabk0919.
CoNi MOF-CNTs	306	J. Mater. Chem. A, 2022, 10, 4936–4943.
Co MOF/CC	346	Small 2021, 17, 2105150.
NiV-MOF NAs	189	Small Methods 2021, 5, 2100573.

Table S3. Comparison of MOF-based catalysts for electrocatalytic HER in 1 M KOH in recent publications.

Catalysts	η_{10} (mV)	Ref.
O_v-Fe MOF/IF	**72**	**This work**
$Ni_3(Ni_3{\cdot}HAHATN)_2$	115	Adv. Sci. 2020, 7, 2000012.
$NiRu_{0.13}$-BDC	36	Nat. Commun. 2021, 12, 1369.
FePc@Ni-MOF	334	Inorg. Chem. 2021, 60, 13, 9987–9995.
Fe(OH)x@Cu-MOF	112	Sci. Adv. 2021,7, eabg2580.
Pt/MOF-O	66	J. Am. Chem. Soc. 2021, 143, 16512−16518.
Co-MOF	34	Angew.Chem.2019,131,4727–4732.
Meso-Cu-BTC	89.32	Mater. Res. Express 2020, 7. 114001.
Co-BDC/MoS_2	248	Small 2019, 15, 1805511.
2D Ni-MOF@Pt	102	Nano Lett. 2019, 19, 8447−8453.
NC-1/2-5	372	ACS Appl. Mater. Interfaces 2020, 12, 45987−45996.
Ru@Ni-MOF	22	Angew. Chem.2021,133, 22450 –22456.
CoNi-MOF-PCG	265	Inorg. Chem. Commun. 2021,127, 108525.
Ni-MOF/Ni_2P@EG	132	Nano Energy 2020, 71, 104621.
Ni@Co-MOFs	349	Inorg. Chem. 2021, 60, 13434−13439.

Table S4. Comparison of MOF-based catalysts for electrocatalytic water splitting in 1 M KOH in recent publications.

Catalysts	E_{10} (V)	Ref.
O_v-Fe MOF/IF	**1.51**	**This work**
Fe-doped MOF CuCoSe@HCNFs	1.57	Appl. Catal. B: Environ.2021,293,120209.
CoNiRu-NT	1.47	Adv. Mater. 2022, 34, 2107488.
NiFe-MS/MOF@NF	1.74@50	Adv. Sci. 2020, 7, 2001965.
CC/MOF-$CoSe_2$@$MoSe_2$	1.53	Chem. Eng. J. 2022, 429, 132379.
LIA-Ni-BDC||LIA-MIL-101(Fe)	1.59	Adv. Funct. Mater. 2021, 31, 2102648.
NFN-MOF/NF	1.56	Adv. Energy Mater.2018, 8, 1801065.
Co_3S_4/EC-MOF	1.55	Adv. Mater. 2019, 31, 1806672.
NiFe-MOF	1.6	Nat. Commun. 2017, 8, 15341.
Co-MOF/NF	1.548	Inorg. Chem. 2021, 60, 4047–4057.
NiFeZn-MNS/NF	1.52	Electrochimica Acta, 2019, 318, 957-965.
Fe-Ni@NC-CNTs	1.98@145	Angew.Chem.2018,130,9059–9064.
defect-Ni-MOF	1.5	Small 2020, 16, 1906564.
NiFe-MS/MOF@NF	1.74@50	Adv. Sci. 2020, 7, 2001965.
CoNiRu-NT	1.47	Adv. Mater. 2022, 34, 2107488.
IrO_2@Ir-MOF	1.53	J. Mater. Chem. A, 2020, 8, 25687-25695.
Fe doped MOF CoV@CoO	1.53@20	Nano Energy 2021, 88, 106238.
FeNi(BDC)(DMF,F)/NF	1.58	Appl. Catal. B: Environ. 2019, 258, 118023.
NiFe(dobpdc)/NF	1.59	J. Mater. Chem. A, 2020, 8, 22974–22982.
Ni@CoO@CoMOFC	1.61	J. Mater. Chem. A, 2021, 9, 22597-22602.